Dynamic Server Allocation Under Stochastic Switchover on Time-Varying Links

Hossein Mohammadalizadeh
Hasso-Plattner-Institute
Internet Technologies and Softwarization
Potsdam, Germany
ho.mohammadalizadeh@hpi.de

Holger Karl
Hasso-Plattner-Institute
Internet Technologies and Softwarization
Potsdam, Germany
holger.karl@hpi.de

***Abstract*—Dynamic resource allocation to parallel queues is a cornerstone of network scheduling, yet classical solutions often fail when accounting for the overhead of switching delays to queues with superior link conditions. In particular, system performance is further degraded when switching delays are stochastic and inhomogeneous. In this domain, the myopic, Max-Weight policy struggles, as it is agnostic to switching delays. This paper introduces Adaptive Channel and switch-aware Index (ACI), a non-myopic, frame-based scheduling framework that directly amortizes these switching delays. We first use a Lyapunov drift analysis to prove that backlog-driven ACI is throughput-optimal with respect to a scaled capacity region; then validate ACI's effectiveness on multi-UAV networks with an Free-Space Optical (FSO) backhaul. Finally, we demonstrate how adapting its core urgency metric provides the flexibility to navigate the throughput-latency trade-off.**

I. Introduction

A broad class of communication systems can be cast as dynamic resource allocation to parallel queues subject to *time-varying link conditions* and *inhomogeneous switching delays* [1]. The central challenge is to design a scheduling policy that is both channel-aware (accounting for link conditions) and switch-aware (accounting for switching delays) to ensure system stability and maximize throughput. Existing paradigms, however, often idealize away these difficulties, leaving a gap between theory and the reality of mobile or directional platforms. This work addresses that gap by formalizing a single-server, parallel-queue model that incorporates random, pair-dependent switching delays and time-varying channels. Within this setting, our goal is to develop scheduling policies that balance instantaneous rate against switching delays. To ground this abstract problem, we introduce a practical example from Unmanned Aerial Vehicle (UAV)-assisted FSO communication that exhibits these exact dynamics.

Consider a two-hop UAV-assisted wireless network with an FSO backhaul, comprising a ground station, one *master* UAV, and multiple *slave* UAVs (see fig. 1). In this system, the ground station points an optical beam to the master drone, which acts as a relay, actively steering the beam to a single chosen slave per time-slot. This physical setup directly gives rise to the two central challenges of our model.

First, the link quality is inconsistent. The combination of atmospheric dynamics, platform mobility, and potential blockages—compounded by the mechanical limitations of steering and the slaves' finite receiver Field of View (FOV)—induces the time-varying channel conditions. Second, switching between slaves is not instantaneous. The handover process requires coarse steering with a *gimbal mirror* and fine alignment with a *Fast Steering Mirror* (FSM), resulting in a delay whose duration depends on the slaves' angular separation [2]. This mechanical process is the physical source of the stochastic and inhomogeneous switching delays. This example faithfully

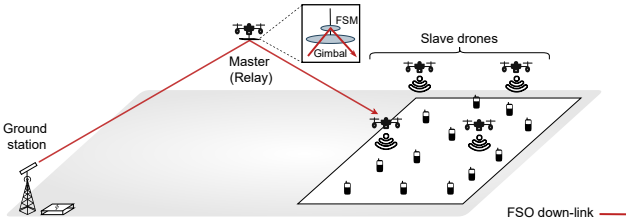

Fig. 1: System model

manifests the structural features of the abstract problem: time-varyting connectivity (stemming from alignment, FOV, and blockage) and inhomogeneous switching (stemming from steering and acquisition). Additionally, the constraint of a single active link makes the choice of scheduling policy important, as it directly dictates network stability and throughput.

Building on this motivation, our contributions are as follows: We (i) provide a concrete system-to-model instantiation that captures the twin challenges of dynamically allocating resources to parallel queues with time-varying connectivity and inhomogeneous switching; (ii) characterize the FSO channel variability and switching statistics induced by actuator dynamics, alignment, and FOV constraints; (iii) we propose and analyze scheduling policies that adapt jointly to channel and switching dynamics and prove throughput optimality—i.e., stabilization of any arrival rate vector strictly within the capacity region under standard ergodicity and finite-moment assumptions; and (iv) validate our approach with simulations.

The authors acknowledge the financial support by the Federal Ministry of Education and Research of Germany in the project "Open6GHub" (grant number: 16KISK011)

II. Related Work

The problem of dynamic server allocation to parallel queues is foundationally addressed by the Max-Weight (MW) algorithm, which is proven to be throughput-optimal when server switching is instantaneous and cost-free [3]. However, in many practical systems, switching server incurs significant time delays. The introduction of such switchover times fundamentally alters the problem, shrinking the stability region and rendering the myopic MW policy sub-optimal, and potentially unstable [4]. Subsequent research has developed switch-overhead-aware policies to address this. One major approach is to amortize the switching cost by committing to a service decision for an extended period. This includes frame-based policies like the FBDC algorithm, which regains asymptotic optimality for fixed switchover delays by using long service dwells [4], and two-timescale policies that separate slow base-station activation from fast user scheduling in wireless networks [5], [6]. A second approach uses hysteresis to suppress inefficient flapping, where the scheduler waits for a state-dependent backlog threshold to be crossed before initiating a switch [7]. These seminal works provide robust solutions but predominantly model switching as a deterministic, uniform delay or an abstract cost penalty therefore they do not fit the scenario in section I, where switching times are state-dependent and stochastic. Our methodology addresses this gap by directly integrating these state-dependent, stochastic switching times into a Lyapunov-based scheduling policy, thereby creating a model that is better aligned with the realities of queuing systems.

III. System Model

A. Queueing Formulation

We study an **M/G/1** queuing system with one server and $|\mathcal{N}|$ parallel queues, each with Markovian arrivals and general service times. Time is slotted into T intervals of length Δt, indexed by t; in each slot the server serves at most one queue. Switching from queue i to j incurs a switching of $\tau_{ij} \in \mathbb{Z}^+$ slots. Let $Q_i(t)$ denote the backlog of queue i at the start of slot t, with Poisson arrivals $A_i(t)$ of rate λ_i and infinite buffers. The server–queue assignment is given by $a_i(t) \in \{0,1\}$ ($1 =$ scheduled), subject to $\sum_{i\in\mathcal{N}} a_i(t) \le 1$ for all t. Server unavailability (due to switching or other outages) is represented by $b(t) \in \{0,1\}$ ($b(t) = 1$ means unavailable), and service eligibility is $e_i(t) = a_i(t)\,(1 - b(t))$. The instantaneous channel rate of queue i in slot t is $R_i(t)$, yielding effective per-slot capacity $\mu_i(t) = \min\{\bar{\mu},\, R_i(t)\}$, where $\bar{\mu}$ is the system throughput cap. Departures and backlog evolve as:

$$D_i(t) = \big(Q_i(t) \wedge \mu_i(t)\big)\, e_i(t), \tag{1}$$

$$Q_i(t+1) = \big(Q_i(t) - D_i(t)\big)^+ + A_i(t), \quad Q_i(0) = 0 \tag{2}$$

with $x \wedge y = \min\{x, y\}$ and $(x)^+ = \max\{x, 0\}$. We model switching delays, $\tau_{ij}(t)$, as *dependent random variables* because, in practice, the time required to switch is not an isolated event. It's influenced by the specific source and destination queues as well as recent switching activity. This approach is superior to modeling the delays as *independent random variables* because it correctly captures how a scheduling policy's choices impact future switching costs. While simpler, the independent model ignores this.

A scheduling policy π selects the next target queue at slot boundaries from the system state:

$$\mathcal{S}(t) \;=\; \big[\,[Q_i(t)]_{i\in\mathcal{N}},\; [R_i(t)]_{i\in\mathcal{N}},\; [\tau_{ij}(t)]_{i\neq j}\,\big] \tag{3}$$

which includes current backlogs, instantaneous channel rates, and pairwise switching delays. The policy induces per-slot decisions $(a_i(t), b(t))$; when switching from i to j, it sets $b(t) = 1$ for $\tau_{ij}(t)$ consecutive slots (so $e_i(t) = 0$ for all i), after which scheduling resumes with $a_j(t) = 1$.

Under a fixed policy with long-run switching frequencies p_{ij} (moves $i \to j$) and average visit lengths v_i, the fraction of slots lost to switching/outages is:

$$\phi_{\text{sw}} \;=\; \frac{\sum_{i\neq j} p_{ij}\, \bar{\tau}_{ij}}{\sum_{k=1}^{N} v_k \;+\; \sum_{i\neq j} p_{ij}\, \bar{\tau}_{ij}} \tag{4}$$

so the usable fraction of time is $1 - \phi_{\text{sw}}$. Each queue i delivers average per-slot service $r_i = \mathbb{E}[\mu_i(t)]$ when connected and is scheduled in a fraction α_i of the usable slots; its effective allocation over all slots is:

$$\varphi_i = (1 - \phi_{\text{sw}})\, \alpha_i \tag{5}$$

$$\varphi_i \ge 0, \qquad \sum_{i=1}^{N} \varphi_i \le 1 - \phi_{\text{sw}} \tag{6}$$

Feasibility of $\Lambda = (\lambda_1, \ldots, \lambda_N)$ requires:

$$\lambda_i < \varphi_i\, r_i, \quad \forall i \tag{7}$$

which yields the compact inner bound:

$$\mathcal{C} \;\supseteq\; \Big\{ \Lambda \in \mathbb{R}_+^N \;:\; \sum_{i=1}^{N} \frac{\lambda_i}{r_i} \;<\; 1 - \phi_{\text{sw}} \Big\} \tag{8}$$

The visit lengths v_i are determined by the load and the chosen scheduling policy. With the preceding queueing formulation and switching-time models, a beam-steered FSO backhaul for a multi-UAV network aligns naturally: per-slot link rates $R_i(t)$ are supplied by the FSO link, while pairwise switching times $\tau_{ij}(t)$ capture beam steering, acquisition, and handover. In the next section we specify the FSO layer that generates $R_i(t)$ and $\tau_{ij}(t)$—including the rate–SNR mapping, and the (time-varying, heterogeneous) switching delays—and couple it to the queuing system above.

B. Network Architecture & FSO Channel Characteristics

The network in fig. 1 comprises a stationary ground station, a fixed master UAV acting as a reflective relay, and $|\mathcal{N}|$ slave UAVs arranged in a large hexagonal pattern. Each slave loiters on a short circular path around its formation point to emulate continuous motion. The end-to-end (E2E) optical gain from

ground to slave i in slot t is a two-hop product through the master, scaled by mirror reflectivity ρ:

$$H_i(t) = \rho\, H_1(t)\, H_{2,i}(t) \tag{9}$$

Each hop $\kappa \in \{1, 2\}$ factors into path loss h_ℓ, atmospheric turbulence h_a, geometric coupling h_g, and pointing loss h_p [8]:

$$H_\kappa(t) = h_{\ell,\kappa}(t)\, h_{a,\kappa}(t)\, h_{g,\kappa}\, h_{p,\kappa}(t). \tag{10}$$

Over a propagation range Z, large-scale attenuation is $h_\ell = \exp(-\xi Z)$ with extinction coefficient ξ. Weak-fluctuation scintillation is modeled as $h_a(t) = \exp(X_t)$ with $X_t \sim \mathcal{N}(\mu, \sigma^2)$, $\mu = -2V$, $\sigma^2 = 4V$, which yields $\mathbb{E}[h_a] = 1$ and controls fading severity via the log-amplitude variance V. The geometric coupling under perfect alignment is:

$$h_g = A_0 = \left[\mathrm{erf}(\nu)\right]^2 \qquad \nu = \frac{\sqrt{\pi}\, a}{\sqrt{2}\, w_z} \tag{11}$$

and the pointing loss for instantaneous radial error $r(t)$ is:

$$h_p(t) = \exp\left(-\frac{2\, r(t)^2}{w_{\mathrm{eq}}^2}\right) \qquad w_{\mathrm{eq}}^2 = w_z^2 \sqrt{\frac{\pi\, \mathrm{erf}(\nu)}{2\nu\, e^{-\nu^2}}} \tag{12}$$

Here, a is the receiving aperture radius and w_z is the gaussian beam radius and ν represents the ratio of the receiver's aperture size to the size of the incoming FSO beam. Hop 1 (ground→master) is static, with Rayleigh radial error $r_1(t)$ and per-axis jitter variance $\sigma_{pg}^2 = \sigma_{p1}^2 + \sigma_g^2$ from the ground transmitter and the master platform. Hop 2 (master→slave) is dynamic; the total error combines lateral displacement ($\delta_{\mathrm{lat}}(t)$) and angular deviation ($\theta_{\mathrm{ang}}(t)$) scaled by the instantaneous range $Z_{2,i}(t)$:

$$r_{2,i}(t) = \delta_{\mathrm{lat}}(t) + Z_{2,i}(t)\, \theta_{\mathrm{ang}}(t) \tag{13}$$

$$\mathrm{Cov}[\delta_{\mathrm{lat}}(t)] = (\sigma_{p1}^2 + \sigma_{p2}^2)\, I_2 \tag{14}$$

$$\mathrm{Cov}[\theta_{\mathrm{ang}}(t)] = \left(4\sigma_{\theta,m}^2 + \sigma_{\theta,2}^2 + \sigma_{\mathrm{turb}}^2\right) I_2 \tag{15}$$

where mirror jitter at the master enters doubled in angle (factor 2; variance factor 4). A hard FOV gate applies: the hop gain is zero if $\|\mathbf{r}_{2,i}(t)\| > Z_{2,i}(t)\theta_{\mathrm{FOV}}$. Table I summarizes hop-specific quantities.

TABLE I: Hop-specific parameters

Parameter	**Hop 1 (Static)**	**Hop 2 (Dynamic)**
Link distance	fixed Z_1	time-varying $Z_{2,i}(t)$
Optics (a, w_z)	$(a_m,\, w_{z,1})$	$(a_r,\, w_{z,2})$
Per-axis jitter	$\sigma_{pg}^2 = \sigma_{p1}^2 + \sigma_g^2$	$\sigma_{\mathrm{lat}}^2 = \sigma_{p1}^2 + \sigma_{p2}^2$
Angular jitter	—	$\sigma_{\mathrm{ang}}^2 = (2\sigma_{\theta,m})^2 + \sigma_{\theta,2}^2$
FOV gate	none	$\|\mathbf{r}_{2,i}(t)\| \le Z_{2,i}(t)\theta_{\mathrm{FOV}}$

The distribution of the E2E gain $H_i(t)$ lacks a closed form due to the product structure and the nonlinear FOV truncation. It is therefore estimated via Monte Carlo simulation of the constituent terms, and the outage probability follows as:

$$P_{\mathrm{out}}(h_{\mathrm{th}}) = \Pr[H_i(t) < h_{\mathrm{th}}] = \int_0^{h_{\mathrm{th}}} f_{H_i}(h)\, dh, \tag{16}$$

with the gain threshold tied to the minimum decoding SNR by:

$$h_{\mathrm{th}} = \frac{\sqrt{\mathrm{SNR}_{\min}}\, \sigma_n}{R \cdot P_t} \tag{17}$$

where R is the detector responsivity, P_t the transmit power, and σ_n the receiver noise standard deviation. The resulting instantaneous data rate for slave i is:

$$R_i(t) = \eta\, B_e \log_2\left(1 + \frac{\mathrm{SNR}_i(t)}{\Gamma}\right) \tag{18}$$

with efficiency η, electrical bandwidth B_e, and SNR gap Γ relative to the Shannon limit. The channel is time-selective, with its coherence time governed by atmospheric turbulence and platform jitter. The atmospheric coherence time, t_0, is given by [9]:

$$t_0 \approx \left[2.91k^2 \int_{\mathrm{path}} C_n^2(h) v(h)^{5/3} dh\right]^{-3/5} \tag{19}$$

where k is the optical wave number, and $C_n^2(h)$ and $v(h)$ are the refractive index and wind speed profiles. As the coherence time of atmospheric effects ($t_0 \approx 10$ ms) is much shorter than that of mechanical platform jitter, turbulence is the dominant factor driving rapid channel fluctuations. This justifies a **block-fading model**, where the channel gain is assumed to be constant over a slot duration Δt on the order of t_0.

C. Stochastic Switching Time Model

Switching the optical beam from a serving slave i to a target slave j is not instantaneous. The total switching time $\mathcal{T}_{ij}(t)$ is a random variable to account for mechanical, electronic, and probabilistic effects. In our example scenario, this time accounts for the sum of the time to re-point the gimbal and FSM and the total time for all link acquisition attempts:

$$\mathcal{T}_{ij}(t) = T_{\mathrm{slew}}(\theta_{ij}) + K \cdot T_{\mathrm{acq}}, \quad \tau_{ij}(t) = \left\lceil \frac{\mathcal{T}_{ij}(t)}{\Delta t} \right\rceil \tag{20}$$

The first term, T_{slew}, is the deterministic mechanical slew time. It is governed by a trapezoidal S-curve velocity profile based on the angular separation θ_{ij} and the gimbal's dynamic limits on maximum velocity ($v_{\max}$), acceleration ($a_{\max}$), and jerk ($j_{\max}$):

$$T_{\mathrm{slew}}(\theta_{ij}) = \frac{\theta_{ij}}{v_{\max}} + \frac{v_{\max}}{a_{\max}} + \frac{4a_{\max}}{j_{\max}} \tag{21}$$

The second term in eq. (20) contains the fixed overhead for a single acquisition attempt, $T_{\mathrm{acq}} = t_{\mathrm{fsm}} + t_{\mathrm{pilot}}$, which includes fine-pointing FSM settling and pilot signal exchange. The total time to establish a link is the number of attempts, K, multiplied by the fixed duration of a single attempt, T_{acq}. We model K as a **geometrically distributed** random variable where the success probability, $p_i(t)$, is dynamic, depending on factors like link distance and pointing accuracy. This model accounts for both **stochastic failures**, where multiple attempts ($K > 1$) increase the delay, and **geometric rejections**, where a link is physically impossible ($p_i(t) = 0$). Since this underlying success probability changes over time, the resulting sequence of switching delays is **temporally correlated**.

IV. Scheduling Approaches

We begin by recalling the classical MW policy. MW is provably throughput-optimal when switching costs are absent [3]; we therefore treat it as a comparison case that captures the best achievable performance in an idealized, no-cost setting. Real systems, however, face inhomogeneous switching delays that MW ignores. To address this gap, we introduce our **Adaptive Channel and switch-aware Index (ACI)** scheduler, which is explicitly designed for settings with stochastic switching delays. We prove that ACI remains throughput-optimal and then develop variations to optimize additional performance objectives under these realistic costs.

A. The Max-Weight Algorithm: A Theoretical Benchmark

The classical MW policy is throughput-optimal for parallel queues *when switching costs are zero*. In our discrete-time model (Sec. III-A), a single server serves queue $i \in \mathcal{N}$ with backlog $Q_i(t)$ and instantaneous service rates $\mu_i(t)$ when connected. At each slot t, MW selects:

$$i^*(t) \in \underset{i\in\mathcal{N}}{\operatorname{argmax}} \left[Q_i(t) \cdot \mu_i(t) \cdot \Delta t\right] \tag{22}$$

This balances backlog and rate and, in the zero-cost case, stabilizes any arrival vector Λ within the capacity region $\mathcal{C}$. Because MW ignores switching delays, applying it with heterogeneous switching delays can trigger frequent handovers and waste service time. This motivates our ACI scheduler developed next.

B. The ACI Scheduling Framework

ACI departs from MW in two ways: (i) it accounts for switching delays in the decision rule, and (ii) it commits to frames of length L instead of single-slot decisions. Frames both amortize the switching delay over L slots and let non-served queues accumulate arrivals (increasing their weights), and reduces oscillations between queues. A switch occurs only when its expected service gain exceeds the switching delay. At each decision point ACI selects queue i^* that maximizes a generalized score:

$$i^*(t) = \underset{i\in N}{\operatorname{argmax}} \left[Q_i(t) \cdot \bar{\mu}_{i|j}(t) \cdot f_{ij}(t)\right] \tag{23}$$

The score is a product of three components. $Q_i(t)$ is the backlog of slave i at time t. $\bar{\mu}_{i|j}(t)$ is the amortized goodput. Ideally, this would be based on the true expected goodput in bits over the frame, $B_i(t; L)$, which requires integrating over future channel rates:

$$B_i(t; L) \triangleq \sum_{\ell=0}^{L-1} R_i(t + \ell\Delta t) \cdot (\Delta t - t_p)^+ \tag{24}$$

Here, Δt is the slot duration and $t_p \in [0, \Delta t)$ is the per-slot processing overhead), so only $(\Delta t - t_p)^+$ seconds per slot are usable. Since future rates $R_i(t + \ell\Delta t)$ are unknown at the decision time t, a practical scheduler must approximate this expectation. We use the current rate $R_i(t)$ as a forecast for the entire dwell:

$$\hat{B}_i(t; L) \approx L \cdot R_i(t) \cdot (\Delta t - t_p)^+ \tag{25}$$

To add robustness, ACI supports *early halt*. Service on the current queue may end before the frame completes when any of the following holds: (i) the queue drains; (ii) the channel is in persistent outage; (iii) the realized rate falls consistently below the forecast used in eq. (25); or (iv) another queue's score in eq. (23) grows sufficiently larger than the current one. Because the score is continuously recalculated, the scheduler can preempt frames when these conditions hold. The amortized goodput is then the initially-estimated total bits, divided by the total time investment (switching time $\tau_{ij}(t)$ and the planned dwell $L \cdot \Delta t$):

$$\bar{\mu}_{i|j}(t) = \frac{\hat{B}_i(t; L)}{\tau_{ij}(t) + L \cdot \Delta t} \tag{26}$$

Finally, ACI provides explicit control via a **Switching Modulator**, $f_{ij}(t)$, which is central to the scheduling decision and is defined as:

$$f_{ij}(t) \triangleq \frac{1 + \gamma \cdot \chi_{ij}(t)}{1 + \beta \cdot \tau_{ij}(t)} \tag{27}$$

This term combines a bonus for *transition affinity*, $\chi_{ij}(t) \in [0, 1]$, with a penalty for the switching duration in slots, $\tau_{ij}(t)$. Transition affinity is a normalized metric that quantifies the efficiency of switching from queue i to j, based on the system's physical or logical structure. For instance, in a network of mobile UAVs where proximity reduces switching time, affinity is physical adjacency. Alternatively, in a system where queues rely on shared software modules, affinity is the degree of resource overlap. The trade-off between these factors is controlled by $\gamma, \beta \geq 0$: increasing γ prioritizes high-affinity switches, while increasing β more heavily penalizes the raw duration to favor faster switchings. For our subsequent optimality proof, we establish its bounds. Given a maximum possible switching duration $\tau_{\max}$, the modulator is bounded, where $f_{\max} = 1 + \gamma$ and $f_{\min} = \frac{1}{1+\beta\tau_{\max}}$.

C. Throughput Optimality of the ACI Scheduler

We prove [1] that ACI is throughput-optimal by showing that the network queues are stable for any arrival rate vector within a scaled version of the capacity region. The proof uses a Lyapunov drift argument over service frames. Let t_k be the start of frame k of duration F_k slots. The one-frame conditional Lyapunov drift, $\Delta_k \triangleq \mathbb{E}[L(Q(t_{k+1})) - L(Q(t_k)) \mid Q(t_k)]$, can be bounded as:

$$\Delta_k \leq B \cdot \mathbb{E}[F_k] + \sum_{i=1}^{N} Q_i(t_k) \left(\Delta t \lambda_i \mathbb{E}[F_k] - \mathbb{E}[\mu_i(k)]\right) \tag{28}$$

where B is a finite constant, λ_i is the arrival rate, and $\mu_i(k)$ is the total service bits delivered to slave i during frame k. The ACI policy can be seen as a practical, switch-aware

[1] See the extended version at [10] for full proofs (An arXiv link will be provided in the final version).

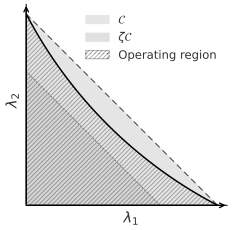

Fig. 2: Capacity region: with switching (ζC) vs without (C)

implementation of the MW principle. Its unscaled objective, $\mathcal{G}_i$ (eq. (23) without switching), is the frame-based equivalent of the MW metric ($Q_i \cdot R_i$). Instead of maximizing this directly, ACI maximizes a scaled version that includes the switching modulator, f_{ij}. The crucial link in the proof is that because the scaling factor $f_{ij} \in [f_{\min}, f_{\max}]$ is bounded, the ACI decision is guaranteed to achieve at least a constant fraction $\zeta \triangleq f_{\min}/f_{\max}$ of the ideal (unscaled) objective. Formally:

$$\mathcal{G}(i^*, L^*) \geq \zeta \cdot \max_{i,L} \mathcal{G}(i, L) \tag{29}$$

This shows that ACI is a constant-factor surrogate for the frame-based MW rule. Recall that MW's throughput optimality applies to the *no-switching* model; with switching, the capacity region contracts to $\zeta\mathcal{C}$. Plugging the interior-point condition $\Lambda \in \text{int}(\zeta\mathcal{C})$ into eq. (28) yields negative drift for sufficiently large backlogs. Equivalently, there exists a feasible service vector $\boldsymbol{\mu} \in \mathcal{C}$ and such that:

$$\lambda_i \leq \zeta\mu_i - \alpha, \quad \forall i \in N \tag{30}$$

Here, $\alpha > 0$ is the slack from the boundary of $\zeta\mathcal{C}$, used to guarantee strictly negative drift. This negative drift condition guarantees bounded queues. Therefore, ACI is throughput-optimal with respect to the scaled capacity region $\zeta\mathcal{C}$, where the factor $\zeta \in (0, 1]$ represents the quantifiable price of incorporating practical switching awareness. Figure 2 shows how switching delays shrink the ideal capacity region $\mathcal{C}$. Since ACI avoids costly switches unless necessary, its operating region for any stabilizable load Λ lies between these two boundaries.

D. ACI Urgency Metric Variations

ACI is flexible, so the backlog term $Q_i(t)$ can be replaced by Head-of-Line (HoL) age to target latency. We consider two variants, **ACI-A (Age-Aware)** with score $\text{Age}_i \cdot \bar{\mu}_{i|j}$ and **ACI-PA (Pure-Age)** with score Age_i only. These variants can reduce latency, yet they are not guaranteed to be throughput-optimal. The backlog-driven ACI is throughput-optimal because the decision weight $Q_i(t)$ aligns with the Lyapunov $L(Q) = \frac{1}{2}\sum_i Q_i^2$ and ensures negative drift under stabilizable load. When backlog is replaced by HoL this alignment disappears, the scheduler may serve a very old packet on a near-zero-rate channel, negative drift is no longer guaranteed, and other queues can grow without bound at high load.

V. Evaluation

We evaluate ACI on a simulated FSO backhaul for multi-UAV networks. Key physical and system parameters are listed in Table II.

TABLE II: Key Simulation Parameters

Symbol	Value	Symbol	Value
N	6	$C_n^2(h)$ Model	HV-5/7
Z_m, Z_s	500 m, 250 m	A_0	1.7e-14 $\text{m}^{-2/3}$
R_{loiter}	150 m	Wind Model	Bufton
Δt	10.41 ms	λ	1.55 µm
L	3 slots	P_t	22 dBm
β, γ	1.0, 1.0	σ_p, σ_θ	0.05 m, 1 mrad
Λ	350 Mbps	θ_{FOV}	9 mrad
$t_{\text{pilot}}, t_{\text{FSM}}$	1 ms, 3 ms	$v_{\max}$	120 deg/s
$a_{\max}$	600 deg/s^2	$j_{\max}$	4000 deg/s^3

As shown in Figure 3, the E2E gain is heavily skewed toward low values, causing frequent outages at modest transmit powers. Thus, we match the slot length to the coherence time to track block fading. The switching delays are stochastic, a

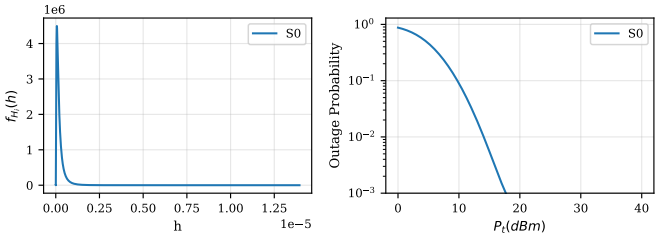

Fig. 3: E2E channel PDF and outage of a single slave

consequence of UAV mobility and beam pointing errors like FOV misses and acquisition failures, as validated in Figure 4 for a representative slave UAV.

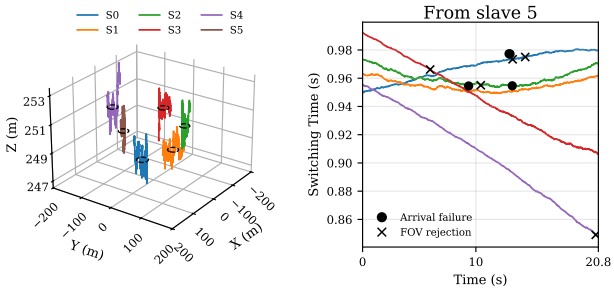

Fig. 4: Slave UAV mobility and switching dynamics

To isolate how switching-time uncertainty shapes performance, we hold arrivals, slotting, horizon, and per-slot rates fixed and compare three switch-time models. In the *IID* case, switch times fluctuate around ring-distance means (near/mid/far) with no memory—think "roughly the same cost every time." The *dependent* case introduces AR(1)-type drift at two levels (global and per-target), so the system experiences recognizable fast/slow phases—bursts of cheap or expensive

switches that persist for a while. The *FSO-driven* case mirrors that correlated behavior but adds the realities of optics: geometric FOV misses and probabilistic acquisition retries. Crucially, Figure 5 reports *packet-delivery delay*, not switching time; switching costs affect it *indirectly* by interrupting service and changing when the scheduler chooses to dwell or move. Consistent with this, ACI(FSO) tracks ACI(Dependent) across most quantiles and then separates in the upper tail due to retries and FOV rejections; ACI(IID) is similar near the median and lightest-tailed because it lacks bursts and failures. The age-prioritizing variants compress the tail: ACI-A (channel-aware age) and ACI-PA (pure age) nearly overlap, with ACI-A slightly left-shifted from better tie-breaking when rates differ.

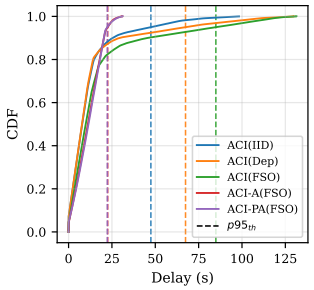

Fig. 5: Overall delay CDF for ACI variants

The time budget in Figure 6 shows the mechanism. A switching-blind Max-Weight chases instantaneous rates, retargets often, and pays a full slew–pilot–settle cycle each time, so wall-clock time is spent switching and service collapses to about 1%. ACI prices switches, rewards adjacency, and commits in short frames, banking dwell until the expected gain exceeds the penalty. As a result, ACI(Dependent) converts about 90% of time into service, while ACI(FSO) remains service-dominant but lower at 75–80% because acquisition retries and FOV misses add overhead. The Dependent–FSO gap is the tax of stochastic acquisition failures beyond pure kinematics.

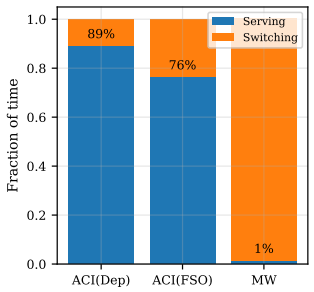

Fig. 6: Fraction of time spent serving vs. switching

To understand each ACI element, we use mean delay as the improvement metric. Figure 7 shows that removing adjacency (longer slews) or the switch penalty (flapping from repeated slew–pilot–settle cycles) raises delay, while the full policy attains the lowest mean delay—evidence that both proximity cues and explicit switch-time pricing are necessary.

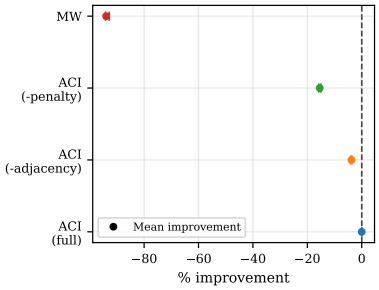

Fig. 7: Effect of ACI components on mean delay (vs. MW)

VI. Summary

We address the problem of dynamic server allocation to parallel queues with stochastic, inhomogeneous switch costs and time-varying connectivity, a problem motivated by FSO backhaul in multi-UAV networks. To overcome the inefficiency of the myopic Max-Weight policy, we propose ACI, a non-myopic, frame-based framework to amortize these switching delays. We prove the backlog-driven ACI is throughput-optimal for a scaled capacity region. Further analysis shows that age-based variants provide superior latency, which reveals a clear performance trade-off: the standard ACI is ideal for maximum throughput, while the channel-aware ACI-A offers the best balance for latency-sensitive applications.

References

[1] L. Tassiulas and A. Ephremides, "Dynamic server allocation to parallel queues with randomly varying connectivity," *IEEE Transactions on Information Theory*, vol. 39, no. 2, pp. 466–478, 1993.

[2] Q. Li, L. Liu, X. Ma, S.-L. Chen, H. Yun, and S. Tang, "Development of multi-target acquisition, pointing, and tracking system for airborne laser communication," *IEEE Transactions on Industrial Informatics*, vol. 15, no. 3, pp. 1720–1729, 2019.

[3] L. Tassiulas and A. Ephremides, "Stability properties of constrained queueing systems and scheduling policies for maximum throughput in multi-hop radio networks," *IEEE Transactions on Automatic Control*, vol. 37, no. 12, pp. 1936–1948, 1992.

[4] G. D. Celik, L. B. Le, and E. Modiano, "Dynamic server allocation over time-varying channels with switchover delay," *IEEE Transactions on Information Theory*, vol. 58, no. 9, pp. 5856–5877, 2012.

[5] S. Krishnasamy, P. T. Akhil, A. Arapostathis, S. Shakkottai, and R. Sundaresan, "Augmenting max-weight with explicit learning for wireless scheduling with switching costs," in *IEEE INFOCOM 2017 - IEEE Conference on Computer Communications*, 2017, pp. 1–9.

[6] S. Basu and S. Shakkottai, "Switching constrained max-weight scheduling for wireless networks," in *IEEE INFOCOM 2019 - IEEE Conference on Computer Communications*, 2019, pp. 2314–2322.

[7] C. W. Chan, M. Armony, and N. Bambos, "Maximum weight matching with hysteresis in overloaded queues with setups," *Queueing System*, vol. 82, no. 3-4, pp. 315–351, Apr. 2016.

[8] M. T. Dabiri, S. M. S. Sadough, and M. A. Khalighi, "Channel modeling and parameter optimization for hovering uav-based free-space optical links," *IEEE Journal on Selected Areas in Communications*, vol. 36, no. 9, pp. 2104–2113, 2018.

[9] A. Tokovinin, A. Kellerer, and V. Coudé Du Foresto, "FADE, an instrument to measure the atmospheric coherence time," vol. 477, no. 2, pp. 671–680, Jan. 2008.

[10] H. Mohammadalizadeh and H. Karl, "Dynamic server allocation under stochastic switchover on time-varying links," https://github.com/ITSW-HPI/ACI, 2025.